

TetraSphere: A Neural Descriptor for O(3)-Invariant Point Cloud Classification

Pavlo Melnyk, Andreas Robinson, Mårten Wadenbäck, Michael Felsberg

Computer Vision Laboratory, Department of Electrical Engineering, Linköping University, Sweden

{pavlo.melnyk, andreas.robinson, marten.wadenback, michael.felsberg}@liu.se

Abstract

Rotation invariance is an important requirement for the analysis of 3D point clouds. In this paper, we present a learnable descriptor for rotation- and reflection-invariant 3D point cloud classification based on recently introduced steerable 3D spherical neurons and vector neurons. Specifically, we show that the two approaches are compatible, and we show how to apply steerable neurons in an end-to-end method for the first time. In our approach, we perform TetraTransform—which lifts the 3D input to an equivariant 4D representation, constructed by the steerable neurons—and extract deeper rotation-equivariant features using vector neurons, subsequently computing pair-wise O(3)-invariant inner products of these features. This integration of the TetraTransform into the VN-DGCNN framework, termed **TetraSphere**, is used to classify synthetic and real-world data in arbitrary orientations. Taking only 3D coordinates as input, TetraSphere sets a new state-of-the-art classification performance on randomly rotated objects of the hardest subset of ScanObjectNN, even when trained on data without additional rotation augmentation. Our results reveal the practical value of spherical decision surfaces for learning in 3D Euclidean space.

1. Introduction

Automatic processing of 3D data obtained with sensors such as LIDARs, sparse stereo, and sparse time-of-flight is a central problem for many autonomous systems [18, 12, 34]. Point clouds—in the form of an array of a fixed number of 3D coordinates and corresponding optional features (e.g., color or intensity)—are a common representation of such data in various 3D vision tasks.

Consider, for example, the task of 3D object classification, where the goal is to predict the correct class given a point cloud. Importantly, the order of the points and different orientations of the shape do not alter its class membership. This imposes the requirements of permutation and rotation invariance on the classifier. Furthermore, in certain real-world scenarios (such as left- and right-hand traffic), global reflection

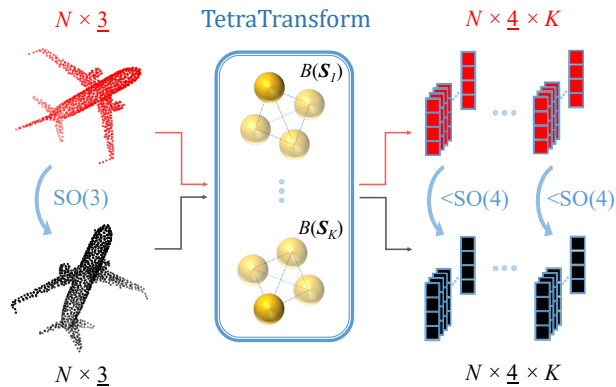


Figure 1. Key component in our method (best viewed in color): a learnable $SO(3)$ -equivariant TetraTransform layer consisting of steerable 3D spherical neurons [28] that lifts the input 3D points to equivariant 4D representations (see Section 4.1 for details).

tion invariance is desired. For instance, a vehicle designed for either type of traffic may be considered the same.

Fulfilling the first requirement is commonly done by constructing a model using shared multilayer perceptrons (MLPs) and a global aggregation function, producing permutation-invariant features, as in, e.g., PointNet [32].

To attain rotation invariance [40], a common approach is to augment available data by performing random rotations and training the model in the hope that it can generalize to other, possibly unknown, orientations during inference. However, such an approach relies heavily on augmentation and requires an increased model capacity. Such methods are commonly referred to as rotation-variant (rotation-sensitive), e.g., [33, 41].

There are also rotation-equivariant methods [43, 38, 9], in which the learned features rotate correspondingly with the input, and rotation-invariant (RI) techniques [47, 24, 5, 7, 16], in which the central trend is to construct RI low-level geometric features and use them instead of point coordinates. An alternative approach is to compute a canonical pose and then de-rotate the input point cloud and perform processing on it [11, 37, 22].

Our method is a combination of $SO(3)$ -equivariant steer-

able 3D spherical neurons [28] and VN-MLPs [9], where deep rotation-equivariant features are learned using vector neurons and invariant predictions are obtained by taking the inner product of these features *point-wise*. However, unlike the original SO(3)-equivariant framework [9], we propagate equivariant features through the network by constructing a specific 4D space spanned by what we call a *tetra-basis*, as shown in Figure 1. Our main hypothesis is that features from learned rotation-equivariant *TetraTransform* projections are more expressive than the points themselves.

We summarize our contributions as follows:

- (1) We identify the compatibility of vector neurons [9] and steerable 3D spherical neurons [28], and propose TetraSphere—a learnable O(3)-invariant descriptor for 3D point cloud classification, built upon VN-DGCNN [9].
- (2) We unveil the practical utility of the steerable neurons, which, to the best of our knowledge, have never previously been used in an end-to-end framework.
- (3) We demonstrate the effectiveness of TetraSphere by using it to classify the most challenging subset of ScanObjectNN [39] real-world data and setting a new state-of-the-art classification performance.

2. Related work

2.1. Rotation-sensitive 3D point cloud learning

PointNet [32] is the pioneering work for learning on raw point sets as input data for the tasks of classification, part segmentation, and semantic segmentation. Its limited ability for recognizing fine-grained patterns was addressed in the PointNet++ method [33] that recursively applies PointNet on a nested partitioning of the input point cloud. Other noteworthy methods include PointCNN [25] with a special type of convolution operator applied to the input points and features before they are processed by an ordinary convolution, and dynamic graph CNN (DGCNN) [41], where a graph convolution is applied to edges of the k -nearest neighbor graph of the point clouds. Xiang *et al.* [45] introduced CurveNet based on a sequence-of-points (curve) grouping operator and a curve aggregation operator. A more geometrically inspired approach was presented by Melnyk *et al.* [27], who revisited modeling spherical decision surfaces with conformal embedding [30] in the context of learning 3D point cloud representations.

Somewhat surprisingly, similar to the projective method for 3D semantic segmentation by Järema Lawin *et al.* [21], it was shown by Goyal *et al.* [14] that on a point cloud classification task, a simple projection-based baseline called SimpleView performs on par with 3D approaches. Moreover, the authors designed a protocol for a fair comparison between point cloud learning methods revealing the importance of many factors orthogonal to the method architectures, such as evaluation procedure and hyperparameter tuning. Re-

cently, a transformer-based approach combining local and global attention mechanisms was presented by Berg *et al.* [1].

Notably, the aforementioned approaches are rotation-variant, i.e., they require data augmentation if rotation invariance is desired. This also entails the model having an increased number of parameters for memorizing the data in various orientations.

2.2. Rotation-aware models

As an alternative, approaches have been proposed for learning rotation equivariant features, in which learned representations rotate in accordance with the input [38, 13, 2, 52, 31, 26]. Among these are quaternion-based models [52, 35] and methods that perform a projection of the 3D input to a unit sphere [8, 10] and realize convolutions in the spherical harmonic domain.

The work of Deng *et al.* [9] introduced *vector neurons* by extending neurons from 1D scalars to 3D vectors, and thereby enabling a simple mapping of SO(3)-actions to latent spaces in the general rotation-equivariant framework. In the context of equivariant methods, Melnyk *et al.* proposed steerable 3D spherical neurons [28], which are SO(3)-equivariant filter banks obtained by virtue of conformal modeling [30, 27] and the symmetries of spheres as geometric entities [28].

Other methods make use of group representation theory and transform the inputs into a space in which it is easier to express rotation-equivariant maps [38, 13, 31], and after that obtain rotation-invariant prediction, e.g., when performing classification. This is achieved using filters constrained to be combinations of spherical harmonics, which limits their expressiveness. Therefore, such methods have naturally limited learning capability, and their performance falls short compared to rotation-sensitive methods for tasks that do not require rotation invariance.

There is a plethora of conceptually different works on hand-crafting low-level RI geometric features for arbitrary pairs of points (PPF) based on angles and distances [48, 51, 47, 7, 17, 16], proposed to be used instead of the input point coordinates. For instance, similar to the triplets used by Granlund *et al.* [15], Zhang *et al.* [49] introduced a convolution operator that uses a point neighborhood constructed with triple-point (reference-neighbor-centroid) local triangles. In contrast, vector norm and relative angles between points were used by Chen *et al.* [3]. A robust RI representation, capturing both local and global shape structures, and region relation convolution, alleviating global information loss, was presented by Li *et al.* [24].

Recently, the pose information loss problem was revealed and addressed by introducing a pose-aware RI convolution (PaRI-Conv) with compact and efficient kernels by Chen and Cong [4]. Therein, a lightweight augmented PPF (APPF)

is proposed, encoding the local pose of each point in a local neighborhood in an ambiguity-free manner. Notably, their approach is also invariant under reflections, i.e., $O(3)$ -invariant, and they use local reference frames (LRFs) as input. However, utilizing principal component analysis (PCA) to construct the LRF for RI point cloud learning, as done by Kim *et al.* [20] and Xiao *et al.* [46], is sensitive to perturbations. This is why Chen and Cong [4] proposed to build the LRFs upon local geometry only.

Input canonicalization is another category of methods that includes both rotation-variant (e.g., variants of [32, 42] that use spatial transformers), -equivariant (e.g., [11, 37, 36]), and -invariant [22] methods. The key idea in these approaches is to bring the input to a computed or predicted canonical reference frame and process it there.

Our approach builds upon the equivariant framework [9]: we apply steerable 3D spherical neurons [28] to learn $SO(3)$ -equivariant 4D features from the 3D input point coordinates and then compute inner product of these features in the equivariant feature space. This way, we create a learnable $O(3)$ -invariant descriptor, encoding both ambiguity-free pose information and local and global context.

3. Preliminaries

In this section, we introduce the necessary notation and recap the notion of equivariance and invariance and theoretical results from prior work, which will enable us to realize the compatibility of steerable 3D spherical neurons and vector neurons.

We define a 3D point cloud $\mathcal{X} \in \mathbb{R}^{N \times (3+C)}$ as a collection of N points, represented by their coordinates $\mathbf{x} \in \mathbb{R}^3$ concatenated with the corresponding optional features $\mathbf{q} \in \mathbb{R}^C$: $\mathcal{X} = \{\mathbf{x}_n \oplus \mathbf{q}_n\}_{n=1}^N$. In the scope of this paper, we focus only on the point coordinates and assume that the optional features are rotation- and reflection-invariant.

3.1. Equivariance and invariance

Given a group G and a set of transformations $T_g : \mathcal{X} \rightarrow \mathcal{X}$ for $g \in G$, a function $f : \mathcal{X} \rightarrow \mathcal{Y}$ is said to be G -equivariant if for every g , there exists a transformation $V_g : \mathcal{Y} \rightarrow \mathcal{Y}$ such that

$$V_g[f(\mathbf{x})] = f(T_g[\mathbf{x}]) \quad \text{for all } g \in G, \mathbf{x} \in \mathcal{X}, \quad (1)$$

where g represents transformation parameters.

Invariance is a particular type of equivariance. A function $f : \mathcal{X} \rightarrow \mathcal{Y}$ is said to be G -invariant if for every $g \in G$, the transformation $V_g : \mathcal{Y} \rightarrow \mathcal{Y}$ is the identity, i.e.,

$$f(\mathbf{x}) = f(T_g[\mathbf{x}]) \quad \text{for all } g \in G, \mathbf{x} \in \mathcal{X}. \quad (2)$$

In particular, we consider invariance under 3D orthogonal transformations (rotations and reflections), i.e., the group

$O(3)$, and, as an intermediate step, equivariance under 3D rotations—the group $SO(3)$. In order to act as a transformation T_g on a 3D vector $\mathbf{x} \in \mathbb{R}^3$, the elements $g \in SO(3)$ are often represented by 3×3 rotation matrices \mathbf{R} [6]. However, this representation is not unique [53].

Our proposed descriptor, which we present in Section 4, is $O(3)$ -invariant and equivariant under permutations of the input points. That is, permuting point indices $1, \dots, N$ results in the corresponding permutation of the descriptor outputs.

In the remainder of the manuscript, we use the same notation to represent a 3D rotation matrix \mathbf{R} in the Euclidean space \mathbb{R}^3 , the projective (homogeneous) space $P(\mathbb{R}^3) \subset \mathbb{R}^4$, and \mathbb{R}^5 , by appending the required number of ones to the diagonal of the original rotation matrix without changing the transformation itself [27].

3.2. Conformal embedding

Geometric transformations are represented in a uniform way in conformal space. Given the Euclidean space \mathbb{R}^n , its conformal counterpart is constructed as $\mathbb{M}\mathbb{E}^n \equiv \mathbb{R}^{n+1,1} = \mathbb{R}^n \oplus \mathbb{R}^{1,1}$, where $\mathbb{R}^{1,1}$ is the Minkowski plane [23]. A Euclidean vector $\mathbf{x} \in \mathbb{R}^n$ is embedded in the conformal space $\mathbb{M}\mathbb{E}^n$ by means of the following non-linear transformation:

$$X = \mathcal{C}(\mathbf{x}) = \mathbf{x} + \frac{1}{2}\|\mathbf{x}\|^2 e_\infty + e_0, \quad (3)$$

where $X \in \mathbb{M}\mathbb{E}^n$ is *normalized* (since the coefficient of e_0 is 1), $\{e_0, e_\infty\}$ is the Minkowski plane $\mathbb{R}^{1,1}$ null basis, representing the origin $e_0 = \frac{1}{2}(e_- - e_+)$ and point at infinity $e_\infty = e_- + e_+$, and $\{e_+, e_-\}$ is an orthonormal basis in $\mathbb{R}^{1,1}$ [23]. Geometrically, the conformal embedding (3) corresponds to a stereographic projection of \mathbf{x} onto a projection sphere in $\mathbb{M}\mathbb{E}^n$ and is *homogeneous*, i.e., all $\mathbb{M}\mathbb{E}^n$ vectors

$$[X] = \{\tilde{X} \in \mathbb{R}^{n+1,1} : \tilde{X} = \gamma X, \gamma \in \mathbb{R} \setminus \{0\}\} \quad (4)$$

represent the same Euclidean vector \mathbf{x} .

The scalar product in the conformal space has an intriguing interpretation in the Euclidean space: given two conformal embeddings X and $Y = \mathbf{y} + \frac{1}{2}\|\mathbf{y}\|^2 e_\infty + e_0$, their scalar product in the conformal space is their (scaled) distance in \mathbb{R}^n , $X \cdot Y = -\frac{1}{2}\|\mathbf{x} - \mathbf{y}\|^2$. This is the key component in the design and implementation of the spherical neurons, which we review in Section 3.3.

For more details, we refer the reader to Li *et al.* [23] and Section 3 in the work of Melnyk *et al.* [27].

3.3. Spherical neurons

Spherical neurons are defined as neurons with (hyper)spherical decision surfaces [30, 27]. Following Perwass *et al.* [30], we embed both a data vector $\mathbf{x} \in \mathbb{R}^n$ and a

hypersphere $S \in \mathbb{MIE}^n$ in \mathbb{R}^{n+2} as

$$\begin{aligned} \mathbf{X} &= (x_1, \dots, x_n, -1, -\frac{1}{2}\|\mathbf{x}\|^2) \in \mathbb{R}^{n+2}, \\ \mathbf{S} &= (c_1, \dots, c_n, \frac{1}{2}(\|\mathbf{c}\|^2 - r^2), 1) \in \mathbb{R}^{n+2}, \end{aligned} \quad (5)$$

where $\mathbf{c} = (c_1, \dots, c_n) \in \mathbb{R}^n$ is the hypersphere center and $r \in \mathbb{R}$ is its radius. Their conformal space \mathbb{MIE}^n scalar product $X \cdot S$ can be equivalently computed in \mathbb{R}^{n+2} as $\mathbf{X}^\top \mathbf{S}$:

$$X \cdot S = \mathbf{X}^\top \mathbf{S} = -\frac{1}{2}\|\mathbf{x} - \mathbf{c}\|^2 + \frac{1}{2}r^2. \quad (6)$$

The sign of this scalar product depends on the relative position of the point to the sphere in the Euclidean space \mathbb{R}^n : inside the sphere if positive, outside of the sphere if negative, and on the sphere if zero [30].

Thus, Perwass *et al.* [30] suggested to use the scalar product (6) as a classifier, i.e., a spherical neuron in \mathbb{MIE}^n is implemented using the standard dot product in \mathbb{R}^{n+2} simply as $f_S(\mathbf{X}; \mathbf{S}) = \mathbf{X}^\top \mathbf{S}$, with learnable parameters $\mathbf{S} \in \mathbb{R}^{n+2}$. Importantly, as noted by Melnyk *et al.* [27], spherical neurons do not necessarily require an activation function, due to the natural non-linearity of the embedding (5).

During training, the components of \mathbf{S} in (5) are treated as independent learnable parameters. Therefore, a spherical neuron effectively learns *non-normalized* hyperspheres of the form $\tilde{\mathbf{S}} = (s_1, \dots, s_{n+2}) \in \mathbb{R}^{n+2}$. Due to the homogeneity (4) of the conformal embedding (3), both normalized and non-normalized hyperspheres represent the same decision surface, and the spherical neuron can thus be written as

$$f_S(\mathbf{X}; \tilde{\mathbf{S}}) = \mathbf{X}^\top \tilde{\mathbf{S}} = \gamma \mathbf{X}^\top \mathbf{S}, \quad (7)$$

where $\gamma := s_{n+2}$ is the (learned) normalization parameter and $\mathbf{S} \in \mathbb{R}^{n+2}$ is the normalized sphere defined in (5). From this point, we will write \mathbf{S} when referring to a spherical decision surface, specifying its normalization if needed.

Further details are found in the work of Melnyk *et al.* [27], where, inter alia, it is demonstrated that the spherical neuron activations are isometries in 3D. That is, rigid transformations commute with the application of the spherical neuron. This result is a necessary condition to design rotation equivariant feature extractors based on spherical neurons [28], that we review in Section 3.4.

3.4. Steerable 3D spherical neurons

Under certain conditions, equivariant operators can be steered. A steerable 3D spherical neuron, recently introduced by Melnyk *et al.* [28], is a filter bank consisting of one learnable spherical decision surface $\mathbf{S} \in \mathbb{R}^5$ (5) and three copies, formed by rotating the original sphere into the other three vertices of the regular tetrahedron, as defined in (8).

To construct this filter bank, the original (learned) sphere center \mathbf{c}_0 is first rotated to $\|\mathbf{c}_0\| (1, 1, 1)$ with the corresponding (geodesic) rotation denoted as \mathbf{R}_O . The resulting sphere is then rotated into the other three vertices of the regular tetrahedron. This is followed by rotating all four spheres back to the original coordinate system. One steerable 3D spherical neuron is thus composed as the 4×5 matrix

$$B(\mathbf{S}) = \left[\mathbf{R}_O^\top \mathbf{R}_{T_i} \mathbf{R}_O \mathbf{S} \right]_{i=0\dots3}, \quad (8)$$

where each of $\{\mathbf{R}_{T_i}\}_{i=0}^3$ is the isomorphism in \mathbb{R}^5 corresponding to a 3D rotation from $(1, 1, 1)$ to the vertex $i + 1$ of the regular tetrahedron. Hence, $\mathbf{R}_{T_0} = \mathbf{I}_5$, i.e., \mathbf{S} remains at \mathbf{c}_0 .

We can view the steerable spherical neuron (8) as a function $f_{4S}(\cdot; \mathbf{S}) : \mathbb{R}^5 \rightarrow \mathbb{R}^4$ with five learnable parameters as a vector \mathbf{S} . Crucially for our work, Melnyk *et al.* [28] proved that it is equivariant under 3D rotations:

$$V_{\mathbf{R}} B(\mathbf{S}) \mathbf{X} = B(\mathbf{S}) \mathbf{R} \mathbf{X}, \quad (9)$$

where $\mathbf{X} \in \mathbb{R}^5$ is a properly embedded 3D input point, \mathbf{R} is a representation of the 3D rotation in the conformal space $\cong \mathbb{R}^5$, and $V_{\mathbf{R}} \in G < \text{SO}(4)$ is the 3D rotation representation in the filter bank output space:

$$V_{\mathbf{R}} = \mathbf{M}^\top \mathbf{R}_O \mathbf{R} \mathbf{R}_O^\top \mathbf{M}, \quad (10)$$

where $\mathbf{M} \in \text{SO}(4)$ is a change-of-basis matrix that holds the homogeneous coordinates of the tetrahedron vertices (scaled by $1/2$) in its columns as

$$\mathbf{M} = \frac{1}{2} \begin{bmatrix} 1 & 1 & -1 & -1 \\ 1 & -1 & 1 & -1 \\ 1 & -1 & -1 & 1 \\ 1 & 1 & 1 & 1 \end{bmatrix}. \quad (11)$$

We will use the equivariant filter bank output as a replacement for 3D points, e.g., in vector neural networks (VNNs) by Deng *et al.* [9].

3.5. Vector neurons

Two important properties of a VNN [9] are that 1) it is $\text{SO}(3)$ -equivariant and produce RI features at the later layers, and 2) the local interaction between the points is modeled by exploiting edges, i.e., edge convolution introduced in DGCNN [41].

Vector neurons (VNs) [9] are designed for processing data embedded in \mathbb{R}^3 and produce an ordered set of 3D vectors $\mathbf{y} \in \mathbb{R}^3$ as output. Taking a point cloud $\mathcal{X} \in \mathbb{R}^{N \times 3}$ as input, a VN extracts vector-list features $\mathcal{Y} = \{\mathbf{Y}_n\}_{n=1}^N \in \mathbb{R}^{N \times C \times 3}$, where $\mathbf{Y} \in \mathbb{R}^{C \times 3}$ is a vector-feature and C is the number of latent channels.

Specifically, a linear layer $f_{\text{lin}}(\cdot; \mathbf{W})$ comprised of VNs is defined by means of a weight matrix $\mathbf{W} \in \mathbb{R}^{C' \times C}$ acting

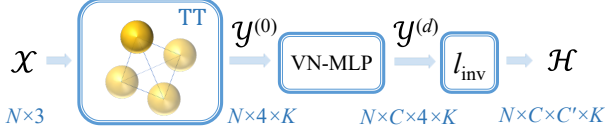


Figure 2. High-level architecture of TetraSphere: the equivariant TT layer (15) is followed by the application of the equivariant VN-MLP, consisting of d VN-layers l_{VN} (16), and the block $l_{\text{inv}}(\cdot; \Theta, \Phi)$ (18), producing invariant features.

on a vector-feature $\mathbf{Y} \in \mathcal{Y}$ as $f_{\text{lin}}(\mathbf{Y}; \mathbf{W}) = \mathbf{W}\mathbf{Y}$, and is $\text{SO}(3)$ -equivariant since

$$f_{\text{lin}}(\mathbf{Y}\mathbf{R}; \mathbf{W}) = \mathbf{W}\mathbf{Y}\mathbf{R} = f_{\text{lin}}(\mathbf{Y}; \mathbf{W})\mathbf{R} = \mathbf{Y}'\mathbf{R}, \quad (12)$$

where $\mathbf{R} \in \text{SO}(3)$ and $\mathbf{Y}' \in \mathbb{R}^{C' \times 3}$.

Deng *et al.* [9] also presented how common neural network operations, such as batch norm [19], pooling, and non-linearities, can be adopted for VNs, and how VNs can be used in other point cloud processing networks. In particular, their VN-DGCNN modifies the permutation-equivariant edge convolution of the predecessor DGCNN [41] by computing adjacent edge features $\mathbf{E}'_{nm} \in \mathcal{E}$ of vector-list representations $\mathbf{Y}_n \in \mathbb{R}^{C \times 3}$, followed by a local $\text{SO}(3)$ -equivariant pooling as

$$\mathbf{E}'_{nm} = l_{\text{VN-nonlin}}(\Theta(\mathbf{Y}_m - \mathbf{Y}_n) + \Phi\mathbf{Y}_n), \quad (13)$$

$$\mathbf{Y}'_n = l_{\text{VN-pool } m:(n,m) \in \mathcal{E}}(\mathbf{E}'_{nm}), \quad (14)$$

where Θ and Φ are learnable weight matrices, VN-nonlin and VN-pool are the respective equivariant non-linear and pooling layers (see Section 3 in Deng *et al.* [9] for details).

Notably, average pooling, being a linear operation, maintains rotation-equivariance and helps to achieve higher performance [9].

4. TetraSphere

In this section, we present TetraSphere—a learnable descriptor for $\text{O}(3)$ -invariant point cloud processing—based on steerable 3D spherical neurons and the VN-framework.

Our overall approach consists of two steps: 1) we extract $\text{SO}(3)$ -equivariant features, and 2) we obtain $\text{O}(3)$ -invariant representations from them. As the first step, we perform TetraTransform (TT), i.e., lift the 3D input to a specific 4D space spanned by what we call a *tetra-basis* (see Figure 1).

Transforming points in the tetra-basis implies embedding a 3D rotation into a subgroup of $\text{SO}(4)$ [28]. Since the entire theory of VNs [9] applies to \mathbb{R}^4 and $\text{SO}(4)$ exactly the same way it does to \mathbb{R}^3 and $\text{SO}(3)$, we plug our TetraTransform into VNs of dimension 4 and achieve rotation invariance. Note, however, that the VN layers operating on 4D vectors in our model are still equivariant only under 3D rotations.

4.1. Learning $\text{SO}(3)$ -equivariant features

TetraTransform The first layer $l^{(0)}$ is formed by the TT layer $l_{\text{TT}}(\cdot; \mathbf{S}) : \mathbb{R}^{N \times 3} \rightarrow \mathbb{R}^{N \times 4 \times K}$, consists of K steerable spherical neurons $B(\mathbf{S}_k)$ (8), representing a $K \times 5$ learnable weight matrix \mathbf{S} .

TT first takes in a point cloud of 3D points $\mathcal{X} \in \mathbb{R}^{N \times 3}$ and embeds them in the conformal space \mathbb{R}^5 according to (5), resulting in $\{\mathbf{X}_n\}_{n=1}^N \in \mathbb{R}^{N \times 5}$.

Following the structure of point cloud processing networks [32, 41], the subsequent application of the steerable spherical neurons (8) is shared across points, thus making the output

$$\mathcal{Y}^{(0)} = l_{\text{TT}}(\mathcal{X}; \mathbf{S}) \in \mathbb{R}^{N \times 4 \times K} \quad (15)$$

both rotation- and permutation-equivariant. Importantly, thanks to the conformal embedding of vectors (5), $l_{\text{TT}}(\cdot; \mathbf{S})$ is a non-linear layer, which is essential for neural networks.

Tetra-basis projections Note that each of the K steerable spherical neurons (8) in $l_{\text{TT}}(\cdot; \mathbf{S})$ has its own representation of a 3D rotation \mathbf{R} , given as $V_{\mathbf{R}}^k \in G < \text{SO}(4)$, $k \in \{1, \dots, K\}$, due to the rotation \mathbf{R}_O in (10) (and (8)) being computed from a learnable \mathbf{S}_k . This must be taken into consideration when transforming $\mathcal{Y}^{(0)}$, especially when obtaining invariant representations. We, therefore, keep all operations in the following sections K -independent. In fact, we see $\mathcal{Y}^{(0)}$ as a collection of N rotation-equivariant 4D vectors in K different tetra-bases.

Deeper equivariant propagation We are free to add more $\text{SO}(3)$ -equivariant layers on top of l_{TT} , if desired. For this, we can use the framework of VNs [9], reviewed in Section 3.5, and apply VNs to the first layer output $\mathcal{Y}^{(0)}$, which we, therefore, need to view as a list of vector-features $\mathcal{Y}^{(0)} = \{\mathbf{Y}_n\}_{n=1}^N \in \mathbb{R}^{N \times 4 \times K}$.

We can thus extend VNs [9] to operate on 4D vectors, such as contained in $\mathcal{Y}^{(0)}$. Obviously, a linear layer comprised of VNs $f_{\text{lin}}(\cdot; \mathbf{W})$ is also equivariant under $V_{\mathbf{R}} \in G < \text{SO}(4)$. By replacing \mathbf{R} in (12) with $V_{\mathbf{R}}$ in (10), and keeping in mind that vector-features \mathbf{Y} contain now 4D vectors, we see that (12) holds. The same applies to other VN-layers (e.g., non-linearities, batch norm) since they are specifically designed to be rotation-equivariant, see Deng *et al.* [9].

We denote a consequent application of $\text{SO}(3)$ -equivariant (and non-linear) edge convolution (13) and pooling (14) layers as $l_{\text{VN}}(\cdot; \Theta, \Phi) : \mathbb{R}^{N \times C \times 4 \times K} \rightarrow \mathbb{R}^{N \times C' \times 4 \times K}$. In general, the d -th VN-layer taking $\mathcal{Y}^{(d)} \in \mathbb{R}^{N \times C \times 4 \times K}$ as input produces an $\text{SO}(3)$ -equivariant and permutation-equivariant feature map

$$\mathcal{Y}^{(d+1)} = l_{\text{VN}}(\mathcal{Y}^{(d)}; \Theta, \Phi) \in \mathbb{R}^{N \times C' \times 4 \times K}, \quad (16)$$

where C' are the latent channels. Given the TT output (15) $\mathcal{Y}^{(0)} \in \mathbb{R}^{N \times 4 \times K}$, a VN-layer outputs a feature map $\mathcal{Y}^{(1)} \in \mathbb{R}^{N \times C \times 4 \times K}$.

4.2. O(3)-invariant representations

The TetraSphere architecture (see Figure 2), presented in this section, performs TT (15) as the first step.

To obtain RI features, we follow related work (e.g., [9] and [47]) and exploit the fact that the inner product of two roto-equivariant vectors, rotated in \mathbb{R}^n with the same \mathbf{R} , is invariant:

$$\mathbf{U}\mathbf{R}(\mathbf{T}\mathbf{R})^\top = \mathbf{U}\mathbf{R}\mathbf{R}^\top\mathbf{T}^\top = \mathbf{U}\mathbf{T}^\top = \mathbf{H}, \quad (17)$$

where $\mathbf{U} \in \mathbb{R}^{C \times n}$, $\mathbf{T} \in \mathbb{R}^{C' \times n}$, and $\mathbf{H} \in \mathbb{R}^{C \times C'}$. Note that \mathbf{H} is $O(n)$ -invariant since the sign of $\det(\mathbf{R})$ does not change the equality (17).

If we take (17) and consider $\mathbf{U} \in \mathbb{R}^{C \times 3}$ and $\mathbf{T} \in \mathbb{R}^{C' \times 3}$ to be 3D vector-features of the same 3D point, but at two different layers with C and C' channels, respectively, we will get the VN-framework approach (see Section 3.5 in Deng *et al.* [9]). In this case, we refer to (17) as a *point-wise* inner product of features. We adopt this procedure to our 4D vectors and perform this for each K .

In the first step, TT (15) produces $\mathcal{Y}^{(0)} \in \mathbb{R}^{N \times 4 \times K}$. We then apply a desired number of VN-layers (16) to it, obtaining $\mathcal{Y}^{(d)} \in \mathbb{R}^{N \times C \times 4 \times K}$.

To produce RI features, we follow Deng *et al.* [9] and concatenate $\mathcal{Y}^{(d)}$ with its global mean (over N), $\bar{\mathcal{Y}}^{(d)} = \frac{1}{N} \sum_n \mathcal{Y}_n^{(d)} \in \mathbb{R}^{C \times 4 \times K}$, and propagate the result through m additional VN-layers to obtain $\mathcal{Y}^{(d+m)} \in \mathbb{R}^{N \times C' \times 4 \times K}$. We then extract matrices $\mathbf{U} \in \mathbb{R}^{C \times 4}$ from $\mathcal{Y}^{(d)}$ and $\mathbf{T} \in \mathbb{R}^{C' \times 4}$ from $\mathcal{Y}^{(d+m)}$ and perform (17) for all N and K .

We denote the propagation from VN-layer d to layer $d+m$ with the subsequent point-wise product as a block $l_{\text{inv}}(\cdot; \Theta, \Phi) : \mathbb{R}^{N \times C \times 4 \times K} \rightarrow \mathbb{R}^{N \times C \times C' \times K}$, where Θ and Φ denote the learnable parameters of the VN-layers. In practice, we select $C' = 4$, motivated by choice of $C' = 3$ in the original VN-approach [9].

In the case of a single VN-layer (16) following after the TT-layer (15), we describe TetraSphere operating on $\mathcal{X} \in \mathbb{R}^{N \times 3}$ as

$$\mathcal{H} = l_{\text{inv}}(l_{\text{VN}}(l_{\text{TT}}(\mathcal{X}; \mathbf{S}))), \quad (18)$$

where $\mathcal{H} \in \mathbb{R}^{N \times C \times C' \times K}$ is an $O(3)$ -invariant and permutation-equivariant descriptor of \mathcal{X} .

TetraSphere encodes densely-connected angle and distance information of 4D vectors. However, it does so on the latent 4D features of each point point-wise, relying on edge convolutions (13) in the VN-layers to model the interaction between the points.

Aggregating over tetra-bases The feature \mathcal{H} (18) is $O(3)$ -invariant, which is why we can safely manipulate its last,

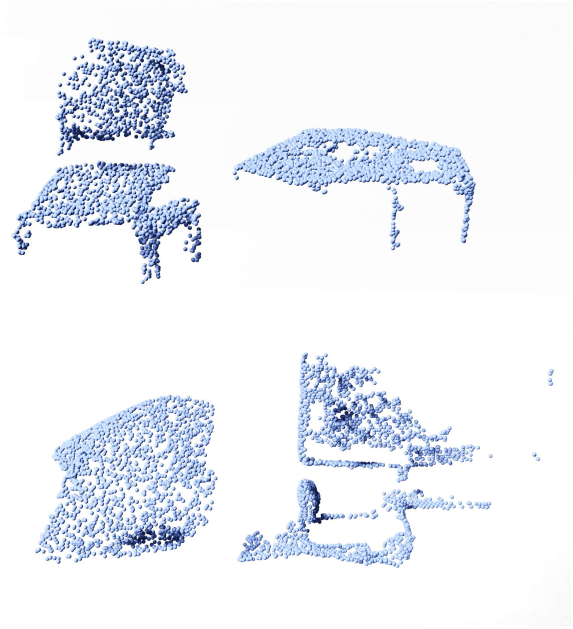


Figure 3. Some examples of the objects from the hardest subset of ScanObjectNN [39]. Top: *chair* and *table*. Bottom: *pillow* and *display*.

tetra-basis, dimension K . While it is possible to combine it with other dimensions, e.g., reshaping the output to be $\mathcal{H} \in \mathbb{R}^{N \times C \times C' \cdot K}$, it will evidently increase the complexity of the model, requiring K times more parameters in the subsequent layer in the network (considering a fully-connected layer).

In this initial study, we will only consider the case $K = 1$ to investigate the practical utility of TetraSphere, which corresponds to a non-linear change of the coordinate system from 3D to a 4D space spanned by the tetra-basis.

5. Experiments

In this section, we conduct experiments with TetraSphere based on the rotation-equivariant VN-DGCNN architecture [9]. We evaluate our model on the task of classifying synthetic and real-world 3D objects and compare it with the results from VN-DGCNN [9] and other methods.

5.1. Datasets

ModelNet40 We use the ModelNet40 dataset [44] provided by [32] that consists of 12,311 CAD models of 40 classes and has been widely employed for the task of synthetic 3D shape classification [4, 52, 24]. The dataset is split into 9843 training shapes and 2468 shapes for testing. We follow the common preprocessing routine and randomly sample 1024 points from each 3D model, center them at the origin, and normalize them to a unit sphere. A shape from the test split can be seen in Figure 1.

Methods	z/z	$z/\text{SO}(3)$	$\text{SO}(3)/\text{SO}(3)$
Rotation-sensitive			
PointNet++ [33]	91.8	28.4	85.0
PointCNN [25]	92.5	41.2	84.5
DGCNN [42]	90.3	33.8	88.6
ShellNet [50]	93.1	19.9	87.8
Rotation-equivariant			
Spherical-CNN [10]	88.9	76.7	86.9
TFN [38]	88.5	85.3	87.6
TFN [31]	89.7	89.7	89.7
VN-DGCNN [9]	89.5	89.5	90.2
TetraSphere (Ours)	90.1	90.1	90.0
Rotation-invariant			
RI-Conv [49]	86.5	86.4	86.4
ClusterNet [3]	87.1	87.1	87.1
RI-Framework [24]	89.4	89.4	89.3
SGMNet [47]	90.0	90.0	90.0
AECNN [48]	91.0	91.0	91.0
3D-GFE [7]	88.6	89.4	89.0
LGANet [17]	90.0	90.0	90.0
Li <i>et al.</i> [22]	91.6	91.6	91.6
PaRINet [5]	91.4	91.4	91.4
ELGANet [16]	90.3	90.3	90.3

Table 1. Classification accuracy (%) on the ModelNet40 shapes under different train/test settings of rotation augmentation. The listed methods use no additional input information, such as normals or features. The best results per method category are presented in **bold**.

ScanObjectNN We also evaluate our method on real-world indoor scenes. For this, we use ScanObjectNN [39], which consists of approximately 15,000 objects with 2902 unique objects instances belonging to 15 classes. We employ its hardest subset called PB_T50_RS, in which perturbations introduce various levels of partiality and background to the objects. Besides, the objects undergo 50% bounding box translation, random rotation around the gravity axis, and random scaling. Some examples are presented in Figure 3.

We preprocess the dataset the same way as ModelNet40, obtaining 1024 points per object instance, and follow the train/test split provided by the original repository¹.

Rotation setup In general, we employ the following train/test rotation settings: $I/\text{SO}(3)$, z/z , $z/\text{SO}(3)$ and $\text{SO}(3)/\text{SO}(3)$, with the first one being the most challenging and the most practical. Here, “I” means no rotation augmentation, z denotes vertical-axis rotation augmentation, and $\text{SO}(3)$ stands for arbitrary 3D rotations, all generated and applied to the input shapes during training/testing.

¹<https://github.com/hkust-vgd/scanobjectnn>

Methods	$z/\text{SO}(3)$	$\text{SO}(3)/\text{SO}(3)$
PointNet++ [33]	17.2	61.7
PointCNN [25]	17.4	50.9
DGCNN [42]	20.8	63.9
3D-GFE [7]	72.7	73.5
LGANet [17]	73.5	73.5
ELGANet [16]	74.2	74.3
TetraSphere (Ours)	77.0	78.0

Table 2. Classification accuracy (%) on the real-world objects from the PB_T50_RS subset of ScanObjectNN under different train/test settings of rotation augmentation. The listed methods only use 3D coordinates as input. The overall best results are presented in **bold**.

5.2. Architecture and implementation details

We use VN-DGCNN as the backbone, with the standard choice of $k = 20$ (nearest-neighbor graph computation parameter) for all layers and the dropout in the last two fully-connected layers of 0.5. Thus, the VN-MLP and the l_{inv} -block in TetraSphere (see Figure 2) reformulate the structure of the baseline [9]. We apply VN-LeakyReLU as the learnable equivariant non-linearity in (13), and use average pooling in VN-layers (14), given its better performance for the baseline. We refer to the resulting model with $K = 1$ simply as TetraSphere.

We adopt the official implementation of Deng *et al.* [9] to implement our model in PyTorch [29]. Following Melnyk *et al.* [28], we initialize the parameters in the TT layer (i.e., the spheres) using the standard initialization for the linear layers in PyTorch.

We use the same strategy for training TetraSphere as the baseline [9]: We employ SGD with an initial learning rate of 0.1 and momentum equal to 0.9, and a cosine annealing strategy for gradually reducing the learning rate to 0.001. Like the baseline, we augment the data with random translation in the range $[-0.2, 0.2]$ and scaling in the range $[2/3, 3/2]$ during training. For ModelNet40 classification, we train TetraSphere for 250 epochs, and for 1000 epochs for all ScanObjectNN experiments. The batch size is set to 32.

5.3. Results

The main results of our experiments are presented in Table 1 and Table 2, where for a fair comparison, we list methods that only use point clouds/meshes as input, and no additional information, such as normals or features.

TetraSphere is slightly outperformed by some recent RI methods [48, 22, 4] classifying the synthetic ModelNet40 data, as shown in Table 1. On the other hand, TetraSphere respects rotation equivariance, which broadens its applicability; among equivariant methods, including the baseline VN-DGCNN, TetraSphere demonstrates superior performance. The marginally inferior result under the $\text{SO}(3)/\text{SO}(3)$ protocol indicates that our method does not benefit from additional

Methods	I/I	I/ SO(3)	I/O(3)
learnable TT	77.8	77.8	77.8
fixed TT	77.2	77.2	77.2

Table 3. TetraSphere classification accuracy (%) on ScanObjectNN PB_T50_RS objects under three train/test transformation settings. The I/ SO(3) setting is the most appropriate to test the rotation invariance of a method.

rotation augmentation when classifying synthetic shapes.

Classifying the real-world objects from the most challenging subset of ScanObjectNN (see Table 2), our model outperforms the most recent best result [16] by 2.8% under the more practical $z/$ SO(3) protocol, and by 3.7% under the SO(3)/ SO(3) setting, achieving state-of-the-art classification performance.

We also verify that TetraSphere is exactly O(3)-invariant by applying random reflections during inference, as shown in Table 3. Note that even when training on data in a single orientation (“I”), TetraSphere achieves remarkably high performance classifying arbitrarily rotated objects.

Furthermore, we do an ablation study testing the importance of training the TT layer parameters. As presented in Table 3, having a learnable TT (the default choice) results in higher accuracy than when keeping the initial parameters of TT frozen.

5.4. Visualization

The TetraTransform layer l_{TT} (15) parameters have a lucid geometric meaning since they constitute steerable 3D spherical neurons [28] $B(\tilde{S}_k)$ (8), which we illustrate in Figure 4.

For the visualization, we use a ModelNet40 test shape and our TetraSphere with $K = 1$, i.e., a single learnable sphere in l_{TT} , initialized (randomly) as

$$\tilde{S}_{\text{init}} = (-0.0920, 0.2274, 0.0621, -0.0547, 0.1240)$$

and, after the model training is complete, optimized to

$$\tilde{S}_{\text{optim}} = (0.0529, 0.2875, 0.4309, 0.3016, 0.3694).$$

Following Melnyk *et al.* [27], we perform the normalization of the spheres to bring them to the canonical form (5) and extract the centers and radii of S_{init} and S_{optim} :

$$\begin{aligned} \mathbf{c}_{\text{init}} &= (-0.7417, 1.8342, 0.5012), \\ r_{\text{init}} &= 2.2469, \quad \gamma_{\text{init}} = 0.1240, \end{aligned}$$

and

$$\begin{aligned} \mathbf{c}_{\text{optim}} &= (0.1432, 0.7783, 1.1666), \\ r_{\text{optim}} &= 0.5950, \quad \gamma_{\text{optim}} = 0.3694. \end{aligned}$$

The resulting spheres $B(S_{\text{init}})$ and $B(S_{\text{optim}})$ are shown on the top and bottom in Figure 4, respectively.

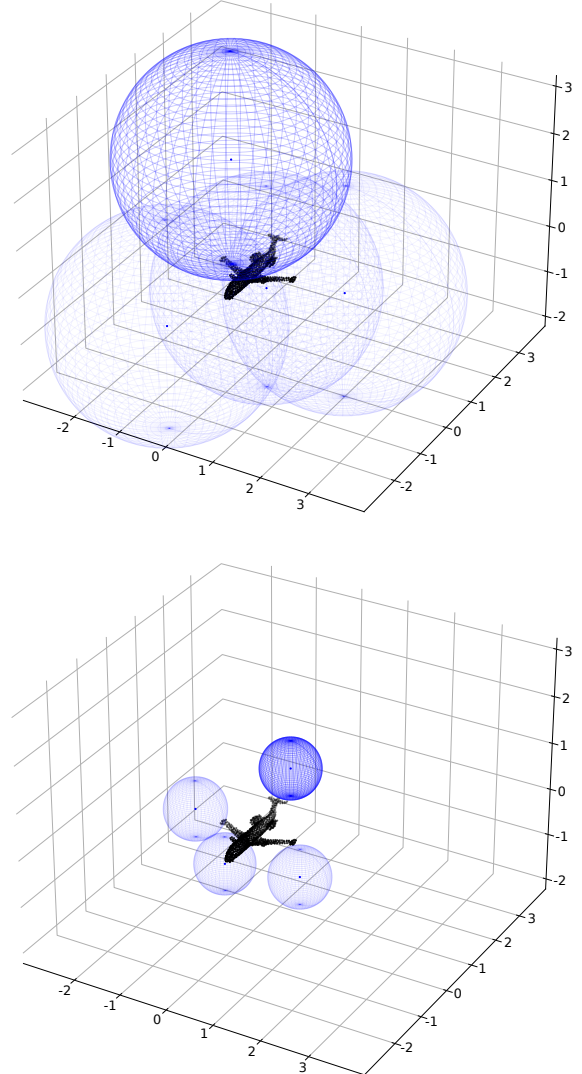


Figure 4. Geometric interpretation of TetraTransform parameters. Top: initial spheres $B(S_{\text{init}})$, with S_{init} highlighted. Bottom: optimized spheres $B(S_{\text{optim}})$ (no sphere intersects with the airplane point cloud), with S_{optim} highlighted.

6. Conclusion

The O(3)-invariant TetraSphere descriptor, proposed in this paper, is based on steerable 3D spherical neurons and builds upon VN-DGCNN. To the best of our knowledge, we use the steerable neurons in an *end-to-end* approach for the first time, thereby unveiling their practical utility. TetraSphere sets a new state-of-the-art performance on the task of classifying randomly rotated 3D objects from the challenging real-world ScanObjectNN dataset. This result demonstrates the effectiveness of spherical decision surfaces for learning in 3D Euclidean space. We believe our work can pave the path to geometrically justified and more robust handling of real-world 3D data.

Acknowledgments

This work was supported by the Wallenberg AI, Autonomous Systems and Software Program (WASP), by the Swedish Research Council through a grant for the project Algebraically Constrained Convolutional Networks for Sparse Image Data (2018-04673), and the strategic research environment ELLIIT. The computations were enabled by resources provided by the Swedish National Infrastructure for Computing (SNIC), partially funded by the Swedish Research Council through grant agreement no. 2018-05973, and by the Berzelius resource provided by the Knut and Alice Wallenberg Foundation at the National Supercomputer Centre.

References

- [1] Axel Berg, Magnus Oskarsson, and Mark O'Connor. Points to patches: Enabling the use of self-attention for 3d shape recognition. In *2022 26th International Conference on Pattern Recognition (ICPR)*, pages 528–534. IEEE, 2022.
- [2] Georg Bökman, Fredrik Kahl, and Axel Flinth. Zz-net: A universal rotation equivariant architecture for 2d point clouds. In *Proceedings of the IEEE/CVF Conference on Computer Vision and Pattern Recognition*, pages 10976–10985, 2022.
- [3] Chao Chen, Guanbin Li, Ruijia Xu, Tianshui Chen, Meng Wang, and Liang Lin. Clusternet: Deep hierarchical cluster network with rigorously rotation-invariant representation for point cloud analysis. In *Proceedings of the IEEE/CVF conference on computer vision and pattern recognition*, pages 4994–5002, 2019.
- [4] Jiayi Chen, Yingda Yin, Tolga Birdal, Baoquan Chen, Leonidas J. Guibas, and He Wang. Projective manifold gradient layer for deep rotation regression. In *Proceedings of the IEEE/CVF Conference on Computer Vision and Pattern Recognition (CVPR)*, pages 6646–6655, June 2022.
- [5] Ronghan Chen and Yang Cong. The devil is in the pose: Ambiguity-free 3d rotation-invariant learning via pose-aware convolution. In *Proceedings of the IEEE/CVF Conference on Computer Vision and Pattern Recognition*, pages 7472–7481, 2022.
- [6] Gregory S Chirikjian. *Engineering applications of noncommutative harmonic analysis: with emphasis on rotation and motion groups*. CRC press, 2000.
- [7] Yu-Chen Chou, Yen-Po Lin, Yang-Ming Yeh, and Yi-Chang Lu. 3d-gfe: a three-dimensional geometric-feature extractor for point cloud data. In *2021 Asia-Pacific Signal and Information Processing Association Annual Summit and Conference (APSIPA ASC)*, pages 2013–2017, 2021.
- [8] Taco S Cohen, Mario Geiger, Jonas Köhler, and Max Welling. Spherical cnns. *arXiv preprint arXiv:1801.10130*, 2018.
- [9] Congyue Deng, Or Litany, Yueqi Duan, Adrien Poulencard, Andrea Tagliasacchi, and Leonidas J Guibas. Vector neurons: A general framework for so (3)-equivariant networks. In *Proceedings of the IEEE/CVF International Conference on Computer Vision*, pages 12200–12209, 2021.
- [10] Carlos Esteves, Christine Allen-Blanchette, Ameesh Makadia, and Kostas Daniilidis. Learning SO(3) Equivariant Representations with Spherical CNNs. In *Proceedings of the European Conference on Computer Vision (ECCV)*, September 2018.
- [11] Jin Fang, Dingfu Zhou, Xibin Song, Shengze Jin, Ruigang Yang, and Liangjun Zhang. Rotpredictor: Unsupervised canonical viewpoint learning for point cloud classification. In *2020 International Conference on 3D Vision (3DV)*, pages 987–996, 2020.
- [12] Hamidreza Fazlali, Yixuan Xu, Yuan Ren, and Bingbing Liu. A versatile multi-view framework for lidar-based 3d object detection with guidance from panoptic segmentation. In *Proceedings of the IEEE/CVF Conference on Computer Vision and Pattern Recognition (CVPR)*, pages 17192–17201, June 2022.
- [13] Fabian Fuchs, Daniel Worrall, Volker Fischer, and Max Welling. Se(3)-transformers: 3d roto-translation equivariant attention networks. In H. Larochelle, M. Ranzato, R. Hadsell, M. F. Balcan, and H. Lin, editors, *Advances in Neural Information Processing Systems*, volume 33, pages 1970–1981. Curran Associates, Inc., 2020.
- [14] Ankit Goyal, Hei Law, Bowei Liu, Alejandro Newell, and Jia Deng. Revisiting point cloud shape classification with a simple and effective baseline. *International Conference on Machine Learning*, 2021.
- [15] Gosta H Granlund and Anders Moe. Unrestricted recognition of 3d objects for robotics using multilevel triplet invariants. *AI Magazine*, 25(2):51–51, 2004.
- [16] Ruibin Gu, Qiuxia Wu, Yuqiong Li, Wenxiong Kang, Wing W. Y. Ng, and Zhiyong Wang. Enhanced local and global learning for rotation-invariant point cloud representation. *IEEE MultiMedia*, 29(4):24–37, 2022.
- [17] Ruibin Gu, Qiuxia Wu, Hongbin Xu, Wing W.Y. Ng, and Zhiyong Wang. Learning efficient rotation representation for point cloud via local-global aggregation. In *2021 IEEE International Conference on Multimedia and Expo (ICME)*, pages 1–6, 2021.
- [18] Hanjiang Hu, Zuxin Liu, Sharad Chitlangia, Akhil Agnihotri, and Ding Zhao. Investigating the impact of multi-lidar placement on object detection for autonomous driving. In *Proceedings of the IEEE/CVF Conference on Computer Vision and Pattern Recognition (CVPR)*, pages 2550–2559, June 2022.
- [19] Sergey Ioffe and Christian Szegedy. Batch normalization: Accelerating deep network training by reducing internal covariate shift. In *International conference on machine learning*, pages 448–456. PMLR, 2015.
- [20] Seohyun Kim, Jaeyoo Park, and Bohyung Han. Rotation-invariant local-to-global representation learning for 3d point cloud. *Advances in Neural Information Processing Systems*, 33:8174–8185, 2020.
- [21] Felix Järemo Lawin, Martin Danelljan, Patrik Tosteberg, Goutam Bhat, Fahad Shahbaz Khan, and Michael Felsberg. Deep projective 3d semantic segmentation. In *International Conference on Computer Analysis of Images and Patterns*, pages 95–107. Springer, 2017.
- [22] Feiran Li, Kent Fujiwara, Fumio Okura, and Yasuyuki Matsushita. A closer look at rotation-invariant deep point cloud analysis. In *Proceedings of the IEEE/CVF International Conference on Computer Vision (ICCV)*, pages 16218–16227, October 2021.
- [23] Hongbo Li, David Hestenes, and Alyn Rockwood. Generalized homogeneous coordinates for computational geometry.

- In *Geometric Computing with Clifford Algebras*, pages 27–59. Springer, 2001.
- [24] Xianzhi Li, Ruihui Li, Guangyong Chen, Chi-Wing Fu, Daniel Cohen-Or, and Pheng-Ann Heng. A rotation-invariant framework for deep point cloud analysis. *IEEE Transactions on Visualization and Computer Graphics*, 2021.
- [25] Yangyan Li, Rui Bu, Mingchao Sun, Wei Wu, Xinhan Di, and Baoquan Chen. PointCNN: Convolution on x-transformed points. *Advances in neural information processing systems*, 31:820–830, 2018.
- [26] Shitong Luo, Jiahua Li, Jiaqi Guan, Yufeng Su, Chaoran Cheng, Jian Peng, and Jianzhu Ma. Equivariant point cloud analysis via learning orientations for message passing. In *Proceedings of the IEEE/CVF Conference on Computer Vision and Pattern Recognition*, pages 18932–18941, 2022.
- [27] Pavlo Melnyk, Michael Felsberg, and Mårten Wadenbäck. Embed me if you can: A geometric perceptron. In *Proceedings of the IEEE/CVF International Conference on Computer Vision (ICCV)*, pages 1276–1284, October 2021.
- [28] Pavlo Melnyk, Michael Felsberg, and Mårten Wadenbäck. Steerable 3D spherical neurons. In *Proceedings of the 39th International Conference on Machine Learning*, volume 162 of *Proceedings of Machine Learning Research*, pages 15330–15339. PMLR, 17–23 Jul 2022.
- [29] Adam Paszke, Sam Gross, Francisco Massa, Adam Lerer, James Bradbury, Gregory Chanan, Trevor Killeen, Zeming Lin, Natalia Gimelshein, Luca Antiga, et al. Pytorch: An imperative style, high-performance deep learning library. In *Advances in Neural Information Processing Systems*, pages 8024–8035, 2019.
- [30] Christian Perwass, Vladimir Banarar, and Gerald Sommer. Spherical decision surfaces using conformal modelling. In *Joint Pattern Recognition Symposium*, pages 9–16. Springer, 2003.
- [31] Adrien Poulenc and Leonidas J. Guibas. A functional approach to rotation equivariant non-linearities for tensor field networks. In *2021 IEEE/CVF Conference on Computer Vision and Pattern Recognition (CVPR)*, pages 13169–13178, 2021.
- [32] Charles R Qi, Hao Su, Kaichun Mo, and Leonidas J Guibas. Pointnet: Deep learning on point sets for 3d classification and segmentation. In *Proceedings of the IEEE conference on computer vision and pattern recognition*, pages 652–660, 2017.
- [33] Charles Ruizhongtai Qi, Li Yi, Hao Su, and Leonidas J Guibas. Pointnet++: Deep hierarchical feature learning on point sets in a metric space. *Advances in neural information processing systems*, 30, 2017.
- [34] Corentin Sautier, Gilles Puy, Spyros Gidaris, Alexandre Boulch, Andrei Bursuc, and Renaud Marlet. Image-to-lidar self-supervised distillation for autonomous driving data. In *Proceedings of the IEEE/CVF Conference on Computer Vision and Pattern Recognition (CVPR)*, pages 9891–9901, June 2022.
- [35] Wen Shen, Binbin Zhang, Shikun Huang, Zhihua Wei, and Quanshi Zhang. 3d-rotation-equivariant quaternion neural networks. In *European Conference on Computer Vision*, pages 531–547. Springer, 2020.
- [36] Riccardo Spezialetti, Federico Stella, Marlon Marcon, Luciano Silva, Samuele Salti, and Luigi Di Stefano. Learning to orient surfaces by self-supervised spherical cnns. *Advances in Neural information processing systems*, 33:5381–5392, 2020.
- [37] Weiwei Sun, Andrea Tagliasacchi, Boyang Deng, Sara Sabour, Soroosh Yazdani, Geoffrey E Hinton, and Kwang Moo Yi. Canonical capsules: Self-supervised capsules in canonical pose. In M. Ranzato, A. Beygelzimer, Y. Dauphin, P.S. Liang, and J. Wortman Vaughan, editors, *Advances in Neural Information Processing Systems*, volume 34, pages 24993–25005. Curran Associates, Inc., 2021.
- [38] Nathaniel Thomas, Tess Smidt, Steven Kearnes, Lusann Yang, Li Li, Kai Kohlhoff, and Patrick Riley. Tensor field networks: Rotation-and translation-equivariant neural networks for 3D point clouds. *arXiv preprint arXiv:1802.08219*, 2018.
- [39] Mikaela Angelina Uy, Quang-Hieu Pham, Binh-Son Hua, Duc Thanh Nguyen, and Sai-Kit Yeung. Revisiting point cloud classification: A new benchmark dataset and classification model on real-world data. In *International Conference on Computer Vision (ICCV)*, 2019.
- [40] Luc Van Gool, Theo Moons, Eric Pauwels, and André Oosterlinck. Vision and lie’s approach to invariance. *Image and vision computing*, 13(4):259–277, 1995.
- [41] Yue Wang, Yongbin Sun, Ziwei Liu, Sanjay E Sarma, Michael M Bronstein, and Justin M Solomon. Dynamic graph cnn for learning on point clouds. *Acm Transactions On Graphics (tog)*, 38(5):1–12, 2019.
- [42] Yue Wang, Yongbin Sun, Ziwei Liu, Sanjay E. Sarma, Michael M. Bronstein, and Justin M. Solomon. Dynamic Graph CNN for Learning on Point Clouds. *ACM Trans. Graph.*, 38(5), oct 2019.
- [43] Maurice Weiler, Mario Geiger, Max Welling, Wouter Boomsma, and Taco S Cohen. 3D steerable CNNs: Learning rotationally equivariant features in volumetric data. In *Advances in Neural Information Processing Systems*, pages 10381–10392, 2018.
- [44] Zhirong Wu, Shuran Song, Aditya Khosla, Fisher Yu, Linguang Zhang, Xiaoou Tang, and Jianxiong Xiao. 3d shapenets: A deep representation for volumetric shapes. In *Proceedings of the IEEE conference on computer vision and pattern recognition*, pages 1912–1920, 2015.
- [45] Tiange Xiang, Chaoyi Zhang, Yang Song, Jianhui Yu, and Weidong Cai. Walk in the cloud: Learning curves for point clouds shape analysis. In *Proceedings of the IEEE/CVF International Conference on Computer Vision (ICCV)*, pages 915–924, October 2021.
- [46] Zelin Xiao, Hongxin Lin, Renjie Li, Lishuai Geng, Hongyang Chao, and Shengyong Ding. Endowing deep 3d models with rotation invariance based on principal component analysis. In *2020 IEEE International Conference on Multimedia and Expo (ICME)*, pages 1–6, 2020.
- [47] Jianyun Xu, Xin Tang, Yushi Zhu, Jie Sun, and Shiliang Pu. SGMNet: Learning rotation-invariant point cloud representations via sorted Gram matrix. In *Proceedings of the IEEE/CVF International Conference on Computer Vision*, pages 10468–10477, 2021.
- [48] Junming Zhang, Ming-Yuan Yu, Ram Vasudevan, and Matthew Johnson-Roberson. Learning rotation-invariant rep-

representations of point clouds using aligned edge convolutional neural networks. In *2020 International Conference on 3D Vision (3DV)*, pages 200–209. IEEE, 2020.

- [49] Zhiyuan Zhang, Binh-Son Hua, David W Rosen, and Sai-Kit Yeung. Rotation invariant convolutions for 3d point clouds deep learning. In *2019 International Conference on 3D Vision (3DV)*, pages 204–213. IEEE, 2019.
- [50] Zhiyuan Zhang, Binh-Son Hua, and Sai-Kit Yeung. ShellNet: Efficient Point Cloud Convolutional Neural Networks Using Concentric Shells Statistics. In *2019 IEEE/CVF International Conference on Computer Vision (ICCV)*, pages 1607–1616, Los Alamitos, CA, USA, nov 2019. IEEE Computer Society.
- [51] Chen Zhao, Jiaqi Yang, Xin Xiong, Angfan Zhu, Zhiguo Cao, and Xin Li. Rotation invariant point cloud classification: Where local geometry meets global topology. *arXiv preprint arXiv:1911.00195*, 2019.
- [52] Yongheng Zhao, Tolga Birdal, Jan Eric Lenssen, Emanuele Menegatti, Leonidas Guibas, and Federico Tombari. Quaternion equivariant capsule networks for 3d point clouds. In *European Conference on Computer Vision*, pages 1–19. Springer, 2020.
- [53] Yi Zhou, Connelly Barnes, Jingwan Lu, Jimei Yang, and Hao Li. On the continuity of rotation representations in neural networks. In *Proceedings of the IEEE/CVF Conference on Computer Vision and Pattern Recognition*, pages 5745–5753, 2019.